Dalton Transactions

Accepted Manuscript

This is an *Accepted Manuscript*, which has been through the RSC Publishing peer review process and has been accepted for publication.

Accepted Manuscripts are published online shortly after acceptance, which is prior to technical editing, formatting and proof reading. This free service from RSC Publishing allows authors to make their results available to the community, in citable form, before publication of the edited article. This *Accepted Manuscript* will be replaced by the edited and formatted *Advance Article* as soon as this is available.

To cite this manuscript please use its permanent Digital Object Identifier (DOI®), which is identical for all formats of publication.

More information about *Accepted Manuscripts* can be found in the **Information for Authors**.

Please note that technical editing may introduce minor changes to the text and/or graphics contained in the manuscript submitted by the author(s) which may alter content, and that the standard **Terms & Conditions** and the **ethical guidelines** that apply to the journal are still applicable. In no event shall the RSC be held responsible for any errors or omissions in these *Accepted Manuscript* manuscripts or any consequences arising from the use of any information contained in them.

Role of different platinum precursors on formation and reaction mechanism of FePt nanoparticles and their electrocatalytic performance towards methanol oxidation

Niroj Kumar Sahu, Anand Prakash and D. Bahadur*

Department of Metallurgical Engineering and Materials Science, Indian Institute of Technology Bombay, Mumbai -400 076, India

Abstract

We report the formation mechanism of FePt nanoparticles (NPs) by high temperature polyol method using equimolar ratio of Fe and Pt-precursor with different Pt-precursors. $Pt(acac)_2$, $PtCl_2$, $PtCl_4$ and $H_2PtCl_6.H_2O$ were used as Pt-precursors and $Fe(acac)_3$ as the only Fe-precursor. Different stoichiometric compositions along with variation in size were obtained by using different precursors of Pt. Nearly, equiatomic FePt having size ~ 2 nm was formed with $Pt(acac)_2$. However, Pt rich phases were formed using all other precursors with size ranging between 3.6 to 6.4 nm. It is found that atomic percentage of Fe in the FePt NPs depends on the reaction parameters. The decomposition behaviour of Fe and Pt-precursors were examined by vibrating sample magnetometer and thermogravimetric measurements. A possible reaction mechanism for Fe depleted FePt formation is proposed which suggests that the reduction potential and decomposition behaviour of the organic and inorganic salts of Pt significantly modify the nucleation behaviour. The electrocatalytic properties of all the four nanomaterials towards methanol oxidation have been investigated by cyclic voltammetry. It is found that $Fe_{19}Pt_{81}$ with an average size of 6.2 nm shows the highest catalytic response.

*Corresponding author: E-mail: dhirenb@iitb.ac.in
Tel: +91 22 2576 7632, Fax: +91 22 2576 3480

1. Introduction

In recent years, the FePt nanoparticles (NPs) systems have received attention for its promising applications in the field of magnetic memory,[1] catalysis[2] and biomedical application[3] because of their tunable magnetic properties, high surface area and Fe leaching behaviour in mild acidic environments. Several synthesis protocols like thermal decomposition,[4] microemulsion,[5] ultrasonication,[6] microwave-assisted,[7] and virus-templated[8] routes are known for the FePt NPs. Among these, thermal decomposition is found to be efficient one due to its capability to control over size, distribution and composition of FePt NPs.[4,9] The growth mechanism for such systems is complicated because these binary compounds are formed through the reduction of metal salts and decomposition of organometallic precursors. Further, it requires control on various factors such as composition and concentration of metallic precursors, stabilizer/surfactant, solvents, reducing agents, reaction temperatures, reaction rates, injection conditions and reaction time etc.[10,11] Lamer *et al.*[12] have suggested that the process of nucleation and growth in solution goes through several stages. However, the control over nucleation and diffusion during growth of FePt NPs is difficult in bi-metallic system due to their mismatch in nucleation rate and difference in the growth process of different metallic precursors. Several articles[9,13] anticipate the two process mechanisms for the synthesis of FePt NPs in high temperature polyol methods in which Pt nucleation occurs in the early stage of reaction (~ 160 ºC) followed by decomposition of Fe precursor (above ~200 ºC). The formation of Fe nuclei by thermal decomposition/reduction of Fe-precursors is assumed to be catalysed by the Pt-nuclei.[14] Jeyadevan *et al.*[15] reported that the reduction potential of the polyols as well as the molar ratio of input polyol to Fe or Pt precursors play crucial role in the nucleation-growth, compositions and the morphology of the FePt NPs. The disordered fcc-FePt structure was explained as the consequence of fast kinetics of the reaction during synthesis.[15,16] Sebt *et* al.[17] mentioned that it is the ligands

(surfactants) which play a crucial role in the synthesis of FePt NPs. They suggested that oleylamine helps to increase the number of NPs in the nucleation stage and decrease the size of the Pt core, whereas the oleic acid controls the shell's growth of the NPs and helps in colloidal stability. Oleylamine is also well known as both reducing agent and stabilizer for synthesis of magnetite NPs.[18,19]

The reaction kinetics of the formation of FePt NPs is still controversial and remains as an unresolved issue. The pioneering work of Sun *et al.*[4] convincingly assured the synthesis of high quality FePt NPs and their application in magnetic recording and exchange couple magnets but the control over composition in FePt systems surfaced as a challenge. Yu and co-workers[20] took this up and investigated the method proposed by Sun *et al.* involving the reduction of $Pt(acac)_2$ and the thermal decomposition of $Fe(CO)_5$ and showed a compositional variation of 21 to 70 at.% Fe from particle to particle. In both the cases $Fe(CO)_5$ was used as the source of Fe which is toxic, volatile and environmentally hazardous. Recently, we have found that an excess of $Fe(CO)_5$ used in the reaction leads to the formation of FePt-Fe_3O_4 core-shell structure giving interesting structural and magnetic properties.[21] Beck *et al.*[14] reported that carbonyl (CO)-spillover process and catalytic activity of Pt nuclei stimulates the complete reduction of hetero-coagulated iron species over the Pt nuclei. This gives a better control over compositional distribution of Fe and Pt among the nanoparticles. Bian *et al.* showed the formation of iron carbonyl and oleylamine complex during the reaction has a strong influence on the nucleation rate and growth process and the resulting shape, size and size distribution of FePt NPs.[22] Saita *et al.*[23] reported the high temperature synthesis (~250-297 ºC) of FePt NPs by allelocatalytic decomposition of precursors and showed that it was dominated by nucleation of Pt followed by a slow growth process of Fe (and Pt) atoms. In order to achieve a good control over the composition and size of NPs, many organic precursors of Fe and Pt have been used.[24,25] To obtain equiatomic FePt NPs, a

higher molar ratio of Fe to Pt precursor is generally used unless a very strong reducing agent like superhydride ($LiBEt_3H$) is used for complete reduction of metallic precursors.[26] To resolve such problems, bimetallic complexes of Fe and Pt with different stoichiometry have been adopted to control the final compositon.[27]

The control over size, its distribution and composition of these FePt systems have raised an overwhelming research interest as a catalyst in the field of fuel cell technology due to the direct conversion of chemical energy into electrical energy with high efficiency and low emission of pollutants.[2,28] The direct methanol fuel cell (DMFC) has emerged as an excellent power source due to its low operating temperature, simplicity of handling and processing of liquid fuels.[29] At present, platinum is the only element which shows significant electrocatalytic activity towards methanol oxidation at relatively lower temperature (90 ºC),[30] but its high cost and finite availability limits its applicability. On the other hand, reaction intermediates like carbon monoxide generated during incomplete oxidation of methanol, adsorbs onto the Pt surfaces and block the active sites thereby deactivation/poisoning the pure Pt.[31] To counter such situations, various intermetallic Pt alloys such as FePt, PtPd, PtRu etc., have been investigated and discussed.[2] However, FePt alloy gains enormous interest due to better CO tolerant and easy availability of Fe over others. The FePt electrocatalyst have more platinum active sites with distinctly different nearest neighbor environments in contrast to pure Pt catalyst.[32] The catalytic activity of FePt in DMFC strongly depends on atomic percentage of Fe and Pt.[33] Therefore, the basic understanding for reaction mechanism of FePt NPs is needed to improve the efficiency of DMFC.

In this context, the key issues in the reaction mechanism of FePt systems are: (i) equimolar ratio of Fe/Pt precursors lead to Fe depleted FePt NPs, (ii) variation in size and composition from particle to particle and (iii) inhomogeneous crystal phase formation (Fe_3Pt or FePt or $FePt_3$). Herein, we have investigated the nucleation of Fe and Pt from their

respective precursors and report the possible reaction mechanism for formation of FePt NPs. The electrochemical activities of as–synthesized FePt NPs towards methanol oxidation have been investigated by cyclic voltammetry. The catalytic efficiency of FePt NPs towards methanol oxidation is found to strongly depend on their composition and size (Scheme-1).

2. Materials and Methods

2.1 Reagents and Materials

Platinum(II) acetylacetonate ($Pt(acac)_2$, Aldrich, 97%), platinum(II) chloride ($PtCl_2$, Aldrich, 98%), platinum(IV) chloride ($PtCl_4$, Aldrich, 98%), chloroplatinic acid hexahydrate ($H_2PtCl_6.6H_2O$, Aldrich, ≥37.5% Pt basis), iron (III) acetylacetonate ($Fe(acac)_3$, Aldrich, 98%), oleylamine (OAm, $C_{18}H_{35}NH_2$, Aldrich, 70%), oleic acid (OAc, $C_{17}H_{33}COOH$, Merck, 70%), 1, 2-hexadecanediol ($C_{16}H_{34}O_2$, Aldrich, 90%), n-hexane (C_6H_{14}, Merck), ethanol (C_2H_6O, Chemical China) and diphenyl ether ($C_{12}H_{10}O$, Aldrich, 99%) were used throughout the reaction for the synthesis of FePt NPs. All chemicals were of analytical grade and were used as received.

2.2 Synthesis Procedure

FePt NPs were prepared by high temperature polyol method. The synthesis was carried out in a three-necked 100 ml flask setup under N_2 atmosphere. In a typical synthesis, $Fe(acac)_3$ (0.2 mmol, 0.071 g), $Pt(acac)_2$ (0.2 mmol, 0.079 g) and 1, 2-hexadecanediol (0.6 mmol, 0.016 g) were dissolved in 20 mL of diphenyl ether. The dissolution was enabled by continuous magnetic stirring (600 rpm) and heating at 120 °C followed by the addition of OAc (0.66 mmol, 0.2 mL) and OAm (0.66 mmol, 0.2 mL). The solution temperature was raised to 200 °C and heated for 2 h. This reaction temperature has been decided by examining the nucleation behaviour of $Fe(acac)_3$ in the above reaction solution through VSM (ESI, Fig-1). Then, it was refluxed for another 1 h at 265 °C. It was found that initial red colour solution turned to black precipitate indicating the formation of FePt NPs. The solution was

allowed to cool to room temperature under N_2 atmosphere. In the post reaction treatment, the black precipitate was washed using 30 mL of ethanol as a flocculent followed by centrifugation (12000 rpm for 10 min) and the reddish supernatant was discarded. The precipitate was dissolved in 5 mL of hexane and two drops (~ 30 µL) of oleylamine. The NPs were again precipitated by the addition of 30 mL of ethanol. The procedure was repeated three times to ensure purification. The black powder was allowed to dry at room temperature for different physical characterizations. For other FePt samples, only Pt precursor ($Pt(acac)_2$) was replaced by $PtCl_2$ (0.2 mmol, 0.053 g), $PtCl_4$ (0.2 mmol, 0.067 g) and $H_2Pt(Cl)_6.6H_2O$ (0.2 mmol, 0.082 g) keeping all other parameters same. The FePt NPs prepared using $Pt(acac)_2$, $PtCl_2$, $PtCl_4$, and $H_2Pt(Cl)_6.6H_2O$ precursor of Pt are labelled as FePt-1, FePt-2, FePt-3 and FePt-4, respectively.

2.3 Characterization techniques

The identification and purity of the phase were confirmed by X-Ray Diffraction (XRD) using Philips powder diffractometer PW3040/60 with Cu K_α radiation (λ = 1.5405 Å) and a Ni filter. The average crystallite size (t) was calculated using the Debye-Scherrer relation. Fourier Transform Infrared (FTIR) spectra of the samples were recorded (Magna 550, Nicolet Instruments Corporation, USA) using KBr pellet as reference. Thermal analysis of the precursors and synthesized samples were carried out in a thermogravimetric-differential thermal analysis instrument (SDT Q100, TA Instruments, USA). The samples were heated from room temperature (RT) to 600 °C at a rate of 10°C/min in nitrogen (N_2) atmosphere. Transmission Electron Microscopy (TEM) images were captured by JEOL JEM-2100F operated at an acceleration voltage of 200 KV. The compositions of the samples were examined by energy dispersive X-ray spectroscopy (EDX) techniques in Field Emission Scanning Electron Microscope (FEG-SEM, JEOL JEM-7600F). The alloy formation is confirmed by scanning tunneling electron microscopy-EDX (STEM-EDX) mapping.

Magnetic properties of the samples were investigated using magnetic properties measurement system (MPMS, Quantum Design, USA). The electrochemical properties of the samples were investigated in a standard three-electrode cell using electrochemical workstation (CHI600D, Austin, TX) at RT. Pt wire was used as a counter electrode, Ag/AgCl (saturated KCl) as a reference electrode and glassy carbon (3 mm diameter) coated with FePt NPs as a working electrode. Prior to the surface coating, the glassy carbon electrode (GCE) was polished using 0.05 mm alumina powders followed by sonication in ethanol and DI water successively (3 times). Further, the electrode was wiped with ethanol and allowed to dry at RT. To fabricate a working electrode, 2 mg of FePt NPs were dispersed in 2 mL of hexane and sonicated for 10 min to get a homogeneous suspension. Then it is drop casted on GCE and air dried before use for methanol oxidation. Electrocatalytic oxidation of methanol was measured in electrolyte containing 0.5 M KOH and 0.5 M CH_3OH by cyclic voltammetry in potential window of -0.2 to 0.6 V with different scan rate. Prior to each measurement, all electrolyte solutions were deaerated by bubbling with N_2 for 30 min.

3. Results and Discussion

3.1 XRD Study

Fig. 1(i) shows the XRD patterns of as-synthesized FePt NPs from different Pt precursors. The XRD patterns of the FePt samples show typical face centred cubic (fcc) structure (JCPDS-29-0717). The observed diffraction planes are indexed with (111), (200), (220) and (311). No peak is observed below 2θ = 40° which arise due to the tetragonal symmetry in chemically ordered face centred tetragonal (fct) FePt NPs. Generally, extra peaks for planes (001), (110), (002), (201), (112) etc. are observed for fct-FePt NPs. This implies that the structures are chemically disordered in nature.[21] The average crystallite sizes estimated from the peak broadening at (111) plane using Scherrer formula are 2.0, 3.4, 4.5 and 4.4 nm for FePt-1, FePt-2, FePt-3 and FePt-4, respectively. The reason behind particle

size variation may be ascribed to difference in the reactivity of the organic and inorganic precursors of platinum. XRD of FePt-1 does not give distinguishable diffraction peaks possibly because of the lower crystallinity and strong surface effects as the size estimated is only 2 nm. A part of XRD pattern is magnified and the Peak shift in the (111) and (200) planes are visible from FePt-1 to FePt-4 (Fig. 1(ii)). This is due to the lattice expansion of FePt NPs with increase in at.% of Pt as the atomic size of Pt (1.39 Å) is more than that of Fe (1.26 Å). This follows the Vegard's Law (Fig.1 (iii)).

3.2 IR Study

Fig. 2 shows the FTIR spectra of oleic acid and oleylamine coated FePt NPs (FePt-1, FePt-2, FePt-3 and FePt-4). The bands at 2854 and 2922 cm^{-1} are assigned to the symmetric (ν_{sym}) and asymmetric (ν_{asym}) CH_2 stretching modes of oleyl group. The band of -C=O stretching mode in -COOH which is supposed to be observed at 1710 cm^{-1}, was not seen. Instead, a low intense peak is observed at 1696 cm^{-1} and that could be due to monodentate link with Fe (-COO-Fe) or free oleic acid. Two new bands are observed at 1540 and 1412 cm^{-1} which are attributed to ($-COO^-$).[34] This confirms the chemical adsorption of oleic acid on the surface of FePt NPs. The difference (Δ = 128 cm^{-1}) between ν_{sym}(COO-) and ν_{asym}(COO-) indicates the bridging bidentate type of covalent bonding.[35] The peak at 3058 cm^{-1} is due to the ν(=CH-) stretching mode of oleic acid/oleyl amine. In cis-configuration, this peak is expected at 3006 cm^{-1} and thus this is assigned to trans-configuration.[34] A broad band centered at 3440 cm^{-1} is a merge of the asymmetric stretching modes of NH_2 of oleylamine and O-H of oleic acid or solvent.[34,36] It may also be possible that the O-H stretching band comes from either due to 1,2-hexadecanediol used in the reaction or due to adsorption of water molecules on the surface of NPs. Absence of 1710 cm^{-1} band (C=O str.) of carboxylic acid and 3300 cm^{-1} (NH_2 str.) of amine group may be due to the formation of acid-base complex ($-COO^-$ and $-NH_3^+$ ions).[34] The peak at 1651 cm^{-1} is assigned to the ν(C=C) stretch

mode of the oleyl group. No peak is observed at 1593 cm^{-1} for bending mode of NH_2 group. It may be due to co-ordination bond formation from lone pair electrons of N in NH_2 to Pt and thus peak is shifted to higher energy (*i.e.* after co-ordination bond formation, the bond energy of NH will increase). Bands below 1500 cm^{-1} arise from complex combinations of the ν (C-C) stretch, ν (C-O) stretches, CH_2 deformations and other lattice vibrations.[14] These observations confirm the surface coating of OAc and OAm over FePt NPs.

3.3 TGA Study

Fig. 3 shows the TGA plots of surfactant mixture (OAc and OAm (1:1 vol. %)) and FePt-1. The surfactant mixture shows nearly 80% of weight loss up to 360 ºC with a weak shoulder near 250 ºC. These features are attributed to the decomposition (or evaporation) of surfactants in the form of CO_2 and water.[37] The TGA of FePt-1 suggests significant weight loss (~ 30%) up to 350 ºC only and confirms the surface coating of FePt NPs with OAc and OAm.[37] The decomposition behaviour of the Fe and Pt precursors has been examined by TGA to understand their nucleation properties (ESI, Fig. S2 and Scheme S1). This indicates that metal organic complexes ($Fe(acac)_3$ and $Pt(acac)_2$) start to decompose below 200 ºC while the decomposition behaviour of $PtCl_2$, $PtCl_4$ and H_2PtCl_6 are complex and found to be in different steps. The different weight loss profiles of Pt-precursors helps in developing the reaction mechanism of FePt systems discussed in next section.

3.4 TEM Study

Fig. 4 shows the TEM images of the as-synthesized FePt NPs. The average diameters are found to be 1.8, 3.6, 6.4 and 6.2 nm for FePt-1, FePt-2, FePt-3 and FePt-4, respectively. The size distributions are almost uniform in case of $Pt(acac)_2$ and $PtCl_2$ with standard deviation (σ) = 0.23 and 0.37 whereas larger particle size with polydispersity is observed in case of $PtCl_4$ and H_2PtCl_6 with σ = 0.64 and 0.63, respectively (Insets of Fig. 4). The lattice spacing of 2.2 Å is the characteristic of (111) planes (ESI, Fig. S3a). The selected area electron

diffraction (SAED) patterns of the samples suggest face-centered cubic structure with good crystallinity except in FePt-1 (ESI, Fig. S3b,c**)**. Here the SAED patterns indicate the chemically disordered fcc structure due to the absence of superlattice diffracted planes ((001), (110), (002) etc.) as that obtained in chemically ordered fct-FePt NPs due to its tetragonal symmetry and superlattice reflections.[21] It may be mentioned that in case of FePt-1, poor diffraction patterns are seen while in all other cases, sharp and similar patterns are obtained. The diffused SAED patterns might be due to the lower crystallinity in FePt-1 NPs.

3.5 Elemental Analysis

Fig. 5a shows the STEM mapping image of FePt-2 NPs. The corresponding EDX profiles of Fe and Pt in the scanned area of the sample show the homogeneity of Fe and Pt throughout the material (Fig.5 b&c). This confirms the formation of alloy NPs. Nearly equiatomic composition of Fe and Pt i.e. $Fe_{46}Pt_{54}$ is formed when $Fe(acac)_3$ and $Pt(acac)_2$ are used as the Fe and Pt–precursors. However, the atomic percentage of Pt is more than Fe suggesting the formation of Fe depleted FePt in other cases. Details of the Fe and Pt elemental analysis of the FePt NPs are listed in Table I. The SEM-EDX spectra of the respective NPs are given in Fig. S4 (ESI). Heller *et al.* reported the formation of $Fe_{19}Pt_{81}$ using equimolar concentration of $Fe(acac)_3$ and $PtCl_2$ by hot injection method.[38] In our synthesis method, $Fe_{32}Pt_{68,}$ $Fe_{25}Pt_{75}$ and $Fe_{19}Pt_{81}$ were formed when $PtCl_2$, $PtCl_4$ and $H_2PtCl_6.6H_2O$, respectively were used as Pt-precursors. The above compositions were obtained by averaging the elemental compositions found by area scanning in SEM-EDX at three different places of the respective NPs.

The formation of Fe-depleted FePt nanoparticle formation can be explained as follows: The reduction potential of Pt^{2+} is 1.18 V ($Pt^{2+} + 2e^- \rightarrow Pt$).[7] This positive reduction potential makes it easy to reduce Pt^{2+} to Pt^0. Due to the lower and positive reduction potential of Pt, it is easily reduced by mild reducing agents like 1,2-hexadecanediol. But this is not true

always. It depends on the type of precursors of Pt (organic/inorganic). The organic precursor of *e.g.* $Pt(acac)_2$ is very facile to reduce than that of $PtCl_2$/ $PtCl_4$/ $H_2PtCl_6.6H_2O$ as suggested from the TGA data and follows a simple one step weight loss profile. On the other hand, the negative reduction potential of Fe (Fe^{2+} + 2e → Fe, V= -0.440V)[7,39] inhibits its ease of reduction. So, its reduction/decomposition requires high temperature or strong reducing agent or their combination. This also depends on the type of Fe-precursor and the reaction medium (aqueous/non-aqueous). Several literature [11,14] explained that Pt nuclei act as a catalyst for the decomposition of Fe salt if it forms at the early stage of reaction. We find that $Pt(acac)_2$ decomposes to Pt at around 150-160 ºC. We believe that when $Fe(acac)_3$ and $Pt(acac)_2$ are used as precursors, equiatomic composition is formed in FePt-1 due to catalytic activity of Pt in the early stage of reaction (~160 ºC) which might help in enhancing the decomposition of $Fe(acac)_3$ to Fe. However, the decomposition of $PtCl_2$/$PtCl_4$/$H_2PtCl_6.6H_2O$ to form Pt occurred at higher temperature (as expected from TGA data) and hence Fe-depleted and Pt rich FePt NPs are formed.

3.6 Magnetic Study

Fig. 6 shows the *M-H* curves of as-synthesized samples (FePt-1, FePt-2, FePt-3 and FePt-4) measured at 300 and 5 K. No hysteresis behaviour is observed at 300K, indicating the superparamagnetic nature. While *M-H* plot of FePt-2, FePt-3 and FePt-4 at 300 K show deviation from linearity and absence of hysteresis indicating the superparamagnetic behaviour, FePt-1, on the other hand, shows linearity in *M* versus *H* indicating a typical paramagnetic nature. However, at 5K, hysteresis is seen for all the samples. The magnetic properties appear to depend on particle size. The magnetisation at H_a=5T increases with increase in the size of the NPs irrespective of composition. This can be interpreted due to reduction in the concentration of surface molecules. Density functional calculations indicate that surface bonding interactions take place predominately at surface of Fe sites which are the

primary contributors to the magnetization in FePt.[40] Further, the superparamagnetic behaviour has been characterized by zero-field cooled (*ZFC*) and field cooled (*FC*) measurements at an applied field of 500 Oe and in the temperature range of 5 to 330 K (Fig. 7). The blocking temperatures (T_B) are found to be varying between 9.2 and 40.3 K and it is directly related to the variation in the particle size of the NPs.[41] Ferromagnetic behaviour has been observed in all FePt NPs at 5 K which is well below T_B. Details of the magnetic data are listed in Table II. The ferromagnetic behaviour at 5K is due to increase in effective anisotropic energy and lowering of thermal energy.[42] The effective magnetic anisotropy constants (K_u) are estimated from the relation K_uV~25 k_BT_B, where V is the volume of the particle, k_B is the Boltzmann constant. The T_B values are taken from table II. The values of K_u are found to be 1.3×10^5, 3.9×10^4, 1.3×10^4 and 1.4×10^4 J/m^3 for FeP-1 to FePt-4, respectively.

4. Electrocatalytic activity of FePt towards methanol oxidation

The electrocatalytic activities of FePt-1, FePt-2, FePt-3 and FePt-4 NPs towards methanol oxidation were characterized by cyclic voltammetry in an electrolyte of 0.5 M KOH having 2 mL of 0.5M CH_3OH with a scanning rate of 50 mV s^{-1} (Fig. 8). The peak position and current intensities were recorded after carrying out 10th cycle. These peaks are generally due to methanol oxidation which gives by-product such as formaldehyde, formic acid and carbon dioxide in the electrolyte solution.[29] Weak peak currents are seen for the FePt-1, FePt-2 and FePt-3 modified GCE electrodes whereas much higher current response is seen for the FePt-4 modified electrode. The cyclic voltammograms of different FePt NPs modified GCE electrodes at successive addition of CH_3OH in the 0.5M KOH are also shown (ESI, Fig. S5). The redox peak currents increases linearly with the successive addition of CH_3OH, indicating that FePt NPs are electroactive towards CH_3OH oxidation. Further, the magnitude of forward anodic peak current (I_f) for FePt-4 is almost one order higher than that of FePt-1, FePt-2 and FePt-3. From the inset of Fig. 8, it is observed that the FePt-1 is slightly more elctroactive

than FePt-2 and FePt-3, though the Pt contained in FePt-1 is lower than the other two. Further, the electrocatalytic activity of FePt-4 is more than the FePt-3, though the particles are of similar sizes. These results indicate that the variation in the ratio of the atomic percentage of Pt to Fe as well as the size of the FePt NPs play important roles in the electrocatalysis. This may be due to the modification in electronic structures of Pt active sites by Fe, interaction of the electrode surface with different size of NPs and/or availability of particles active sites towards the electrolyte. The ratio of forward (I_f) to the backward anodic peak current (I_b) was calculated to evaluate the oxidation efficiency of methanol and the catalyst tolerance to the intermediate carbonaceous species such as CO which has accumulated on the electrode surface. The I_f/I_b ratio for FePt-4 was 5.1 whereas this ratio for FePt-1, FePt-2 and FePt-3 were found to be 7.1, 5.0 and 14.4 respectively. During electrocatalytic methanol oxidation, the observed peaks in backward scan are associated with the oxidation of the carbonaceous intermediates generated via incomplete oxidation. Like forward peaks, the intensities of backward peaks have followed the similar trends. This indicates that more intermediate carbonaceous defects are created for more electroactive FePt nanomaterials. These results suggest that FePt-4 is more electroactive towards methanol oxidation but FePt-3 catalyst has much more tolerance toward carbonaceous intermediate poisoning during oxidation of methanol to carbon dioxide. The effects of scan rates on the redox of methanol at the FePt-modified GCE have been shown in Fig. 9. The reverse peak currents observed in FePt-1, FePt-2 and FePt-3 (Fig. 9) might be related to the reduction of formaldehyde. In contrast, FePt-4 shows oxidative current even at reverse sweep which might be due to the fact that it has good electro-oxidative activity toward formaldehyde. In addition, the redox peak current increases linearly with the scan rate in the range from 10 to 500 mVs^{-1}. This indicates that the FePt modified-electrode reaction of methanol is a surface confined process. More importantly, upon successive increment in voltage scan rate from 10

to 500 mV/s (50 times), the response in forward peak current does not increase prominently. The ratio of forward peak currents at 50 and 500 mV/S is merely 1.44. This confirms that redox process is surface confined and suggests that the active nanomaterials are not fully utilized at very high scan rates because of the concentration polarization, which slows down the diffusion rates of electrolyte ions.[43] More importantly, the slope observed in case of FePt-4 is lowest as compared to other FePt samples. This indicates that methanol oxidation processes observed in case of FePt-4 modified GCE does not depend much on scan rates as compared to other FePt samples. These catalytic activities should not be viewed in terms of performance, but only as the demonstration that FePt-NPs are also effective electrocatalyst.

5. Conclusions

We have synthesized nearly equiatomic FePt NPs using equimolar $Fe(acac)_3$ and $Pt(acac)_2$ precursors by optimising the reaction condition. However, Pt dominated (Fe-depleted) FePt NPs are formed when $PtCl_2$, $PtCl_4$ and $H_2PtCl_6.6H_2O$ are used as Pt-precursors. This may be due to the higher decomposition temperatures of the chloride precursors of Pt. The reduction/decomposition of $Fe(acac)_3$ occurs at around 200 ºC to form Fe nuclei in the absence of Pt nuclei. However, the reduction/decomposition process takes place at an early stage in the presence of Pt nuclei due to its catalytic activity. The size distribution and composition of the FePt NPs significantly changes over different precursors even though all other reaction conditions are kept same. The differences in TGA profiles along with magnetic behaviour give direct information about nucleation and growth. Such studies are useful for understanding the reaction mechanism and formation of FePt NPs. The FePt NPs with suitable composition show significant catalytic properties towards methanol oxidation. The atomic percentage of Pt over Fe as well as the particle size of FePt NPs play crucial role on the catalytic properties.

Supplementary materials

This supplementary materials are available at http://.

Acknowledgement

The financial support from the Nanomission, Department of Science and Technology (DST), Government of India, is gratefully acknowledged. The authors are gratified to the Centre for Research in Nanotechnology & Science (CRNTS), IIT Bombay for TEM & SEM facilities.

References

1. D. Weller and M. F. Doerner, *Annu. Rev. Mater. Sci.,* 2000, **30**, 611-644.

2. V. Mazumder, Y. Lee and S. Sun, *Adv. Funct. Mater.,* 2010, **20**, 1224–1231.

3. C. Xu, Z. Yuan, N. Kohler, J. Kim, M. A. Chung and S. Sun, *J. Am. Chem. Soc.,* 2009, **131**, 15346–15351.

4. S. Sun, C. B. Murray, D. Weller, L. Folks and A. Moser, *Science,* 2000, **287**, 1989-1992.

5. S. Qu, X. W. Zhang, Y. Gao, J. B. You, Y.M. Fan, Z. G. Yin and N. F. Chen, *Nanotechnology*, 2008, **19**, 135704 (1-7).

6. R. D. Rutledge, W. H. Morris, M. S. Wellons, Z. Gai, J. Shen, J. Bentley, J. E. Wittig and C. M. Lukehart, *J. Am. Chem. Soc.,* 2006, **128**, 14210-14211.

7. R. Harpeness and A. Gedanken, *J. Mater. Chem.*, 2005, **15**, 698–702.

8. S. N. Shah, N. F. Steinmetz, A. A. A. Aljabali, G. P. Lomonossoff and D. J. Evans, *Dalton Trans.*, 2009, 8479-8480.

9. C. N. R. Rao, H. S. S. R. Matte, R. Voggua and A. Govindaraja, *Dalton Trans.*, 2012, **41**, 5089-5120.

10. S. Sun, *Adv. Mater.*, 2006, **18**, 393–403.

11. R. Voggu, A. Shireen and C. N. R. Rao, *Dalton Trans.,* 2010, **39**, 6021–6023.

12. V. K. Lamer and R. Dinegar, *J. Am. Chem. Soc*., 1950, **17**, 4847-4854.

13. H. G. Bagaria, D. T. Johnsona, C. Srivastava, G. B. Thompson, M. Shamsuzzoha and D. E. Nikles, *J. Appl. Phys.*, 2007, **101**, 104313(1-3).

14. W. Beck, Jr., C. G. S. Souza, T. L. Silva, M. Jafelicci and L. C. Varanda, *J. Phy. Chem. C*, 2011, **115**, 10475-10482.

15. B. Jeyadevan, K. Shinoda, R. J. Justin, T. Matsumoto, K. Sato, H. Takahashi, Y. Sato and K. Tohji, *IEEE Trans. on Magnetics,* 2006, **42**, 3030-3035.

16. T. Hinotsu, B. Jeyadevan, C. N. Chinnasamy, K. Shinoda and K. Tohji, *J. Appl. Phy.*, 2004, **95**, 7477-7479.

17. S. A. Sebt, S. S. Parhizgar, M. Farahmandjou, P. Aberomand and M. Akhavan, *J Supercond. Nov. Magn.*, 2009, **22**, 849–854.

18. Z. Xu, C. Shen, Y. Hou, H. Gao and S. Sun, *Chem. Mater.*, 2009, **21**, 1778–1780.

19. J. Mohapatra, A. Mitra, D. Bahadur and M. Aslam, *Cryst. Eng. Comm.*, 2013, **15**, 524-532.

20. A. C. C. Yu, M. Mizuno, Y. Sasaki and H. Kondo, *Appl. Phys. Lett.*, 2004, **85**, 6242-6244.

21. N. K. Sahu and D. Bahadur, *J. Appl. Phy.*, 2013, **113**,134303 (1-9).

22. B. Bian, W. Xia, J. Du, J. Zhang, J. P. Liu, Z. Guoc and A. Yana, *Nanoscale*, 2013, **5**, 2454-2459.

23. S. Saita and S. Maenosono, *Chem. Mater.*, 2005, **17**, 6624-6634.

24. Q. Dong, G. Li, C. L. Ho, C. W. Leung, P. W. T. Pong, I. Manners and W. Y. Wong, *Adv. Funct. Mater.* 2013, 1-6, DOI: 10.1002/adfm.201301143.

25. K. Ahrenstorf, H. Heller, A. Kornowski, J. A. C. Broekaert and H. Weller, *Adv. Funct. Mater.*, 2008, **18**, 3850–3856.

26. S. Sun, S. Anders, T. Thomson, J. E. E. Baglin, M. F. Toney, H. F. Hamann, C. B. Murray and B. D. Terris, *J. Phys. Chem. B*, 2003, **107**, 5419-5425.

27. H. M. Song, W. S. Kim, Y. B. Lee, J. H. Hong, H. G. Lee and N. H. Hur, *J. Mater. Chem.*, 2009, **19**, 3677-3681.

28. B. C. H. Steele and A. Heinzel, *Nature*, 2001, **414**, 345-352.

29. A. S. Arico, S. Srinivasan and V. Antonucci, *Fuel Cells*, 2001, **1**, 133-161.

30. F. Colmati, E. Antolini and E. R. Gonzalez, *Electrochim. Acta*, 2005, **50**, 5496.

31. L. C. Nagle and J. F. Rohan, *J. Power Sources*, 2008, **185**, 411-418.

32. W. Li, W. Zhou, H. Li, Z. Zhou, B. Zhou, G. Sun and Q. Xin, *Electrochim. Acta*, 2004, **49**, 1045-1055.

33. W. Chen, J. Kim, S. Sun and S. Chen, *J. Phys. Chem. C*, 2008, **112**, 3891-3898.

34. N. Shukla, C. Liu, P. M. Jones and D. Weller, *J. Mag. Magn. Mater.*, 2003, **266**, 178-184.

35. G. Kataby, M. Cojocaru, R. Prozorov and A. Gedanken, *Langmuir*, 1999, **15**, 1703-1708.

36. G. Chen, H. Qiu, R. Fan, S. Hao, S. Tan, C. Yang and G. Han, *J. Mater. Chem.*, 2012, **22**, 20190- 20196.

37. X. W. Wu, C. Liu, L. Li, P. Jones, R. W. Chantrell and D. Weller, *J. Appl. Phys.*, 2004, **95**, 6810-6812.

38. H. Heller, K. Ahrenstorf, J. A. C. Broekaert and H. Weller, *Phys. Chem. Chem. Phys.*, 2009, **11**, 3257–3262.

39. C. G. Zoski, Handbook of Electrochemistry, *Elsevier, Oxford, UK, First edition*, 2007.

40. G. H. O. Daalderop, P. J. Kelly, and M. F. H. Schuurmans, *Phys. Rev. B*, 1991, **44**, 12054-12057.

41. S. Yoon, and K. M. Krishnan, *J. Appl. Phys.*, 2011, **109**, 07B534(1-3).

42. A. F. Jr. and V. Zapf, *J. Magn. Magn. Mater.*, 2008, **320**, 709–713.

43. M. D. Stoller, S. Park, Y. Zhu, J. An and R. S. Ruoff, *Nano Lett.* 2008, **8**, 3498-3502.

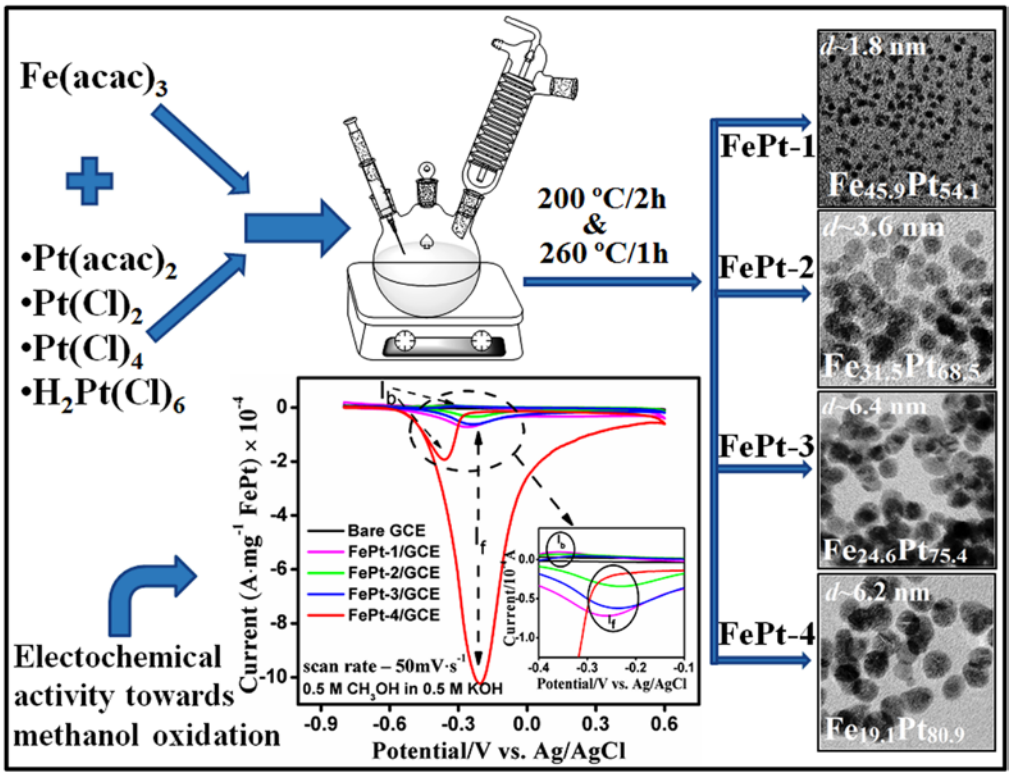

Scheme 1 Schematic representation of the formation of FePt NPs from different platinum precursors and a fixed iron precursor and their electrochemical activity towards methanol oxidation.

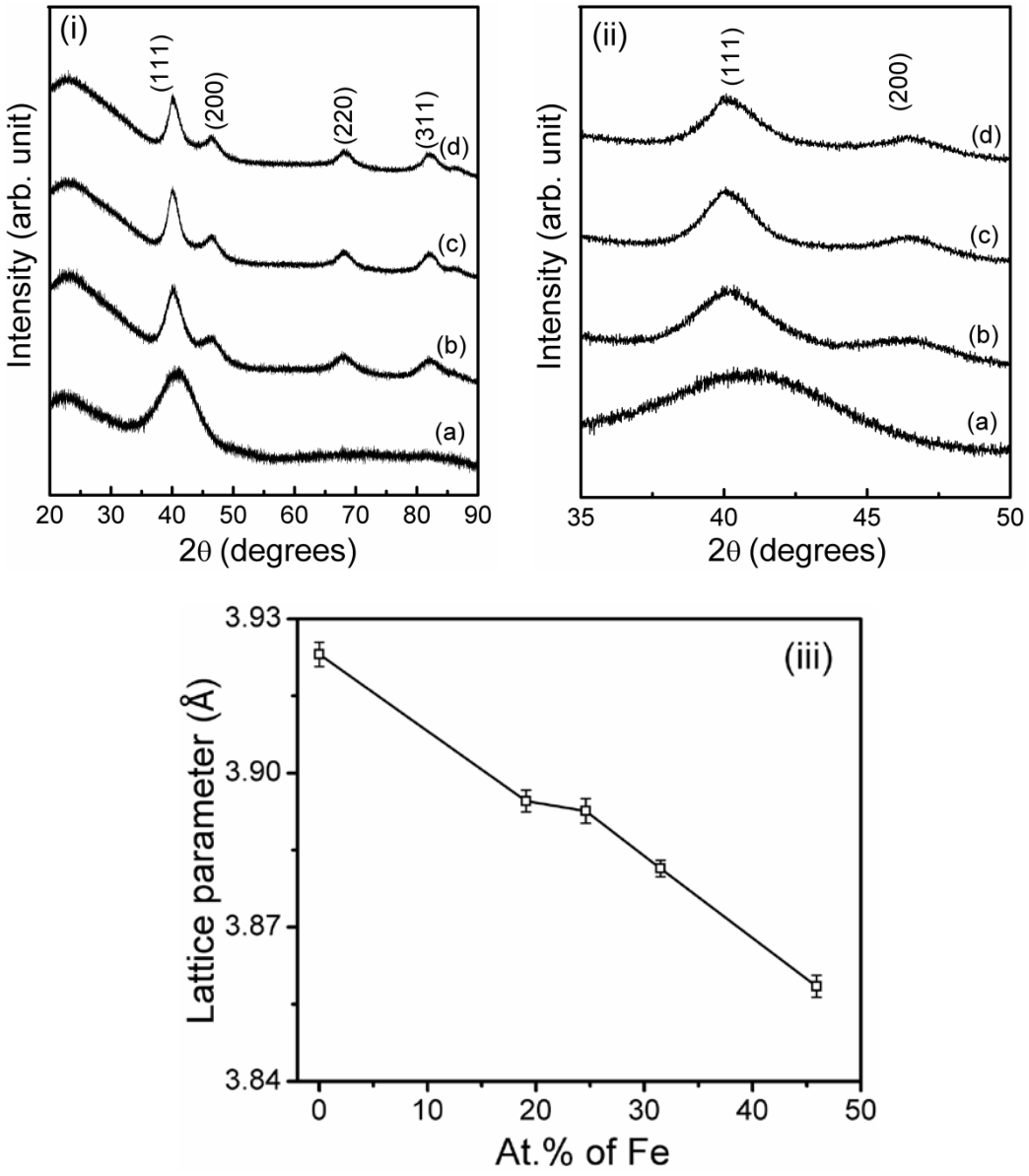

Fig. 1 XRD patterns of (i) as-synthesized FePt NPs: (a) FePt-1, (b) FePt-2, (c) FePt-3, and (d) FePt-4. A part of the patterns is magnified and is shown in (ii). The change in lattice parameter of FePt NPs with the increase in at.% of Fe is shown in (iii).

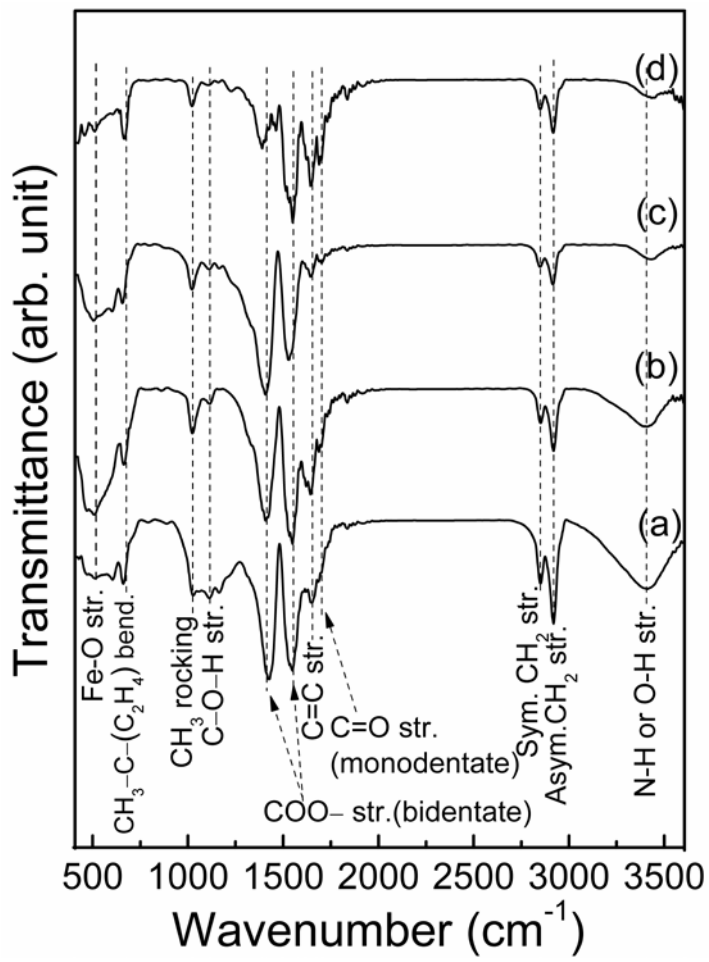

Fig. 2 FTIR spectra of as-synthesized FePt NPs: (a) FePt-1, (b) FePt-2, (c) FePt-3, and (d) FePt-4.

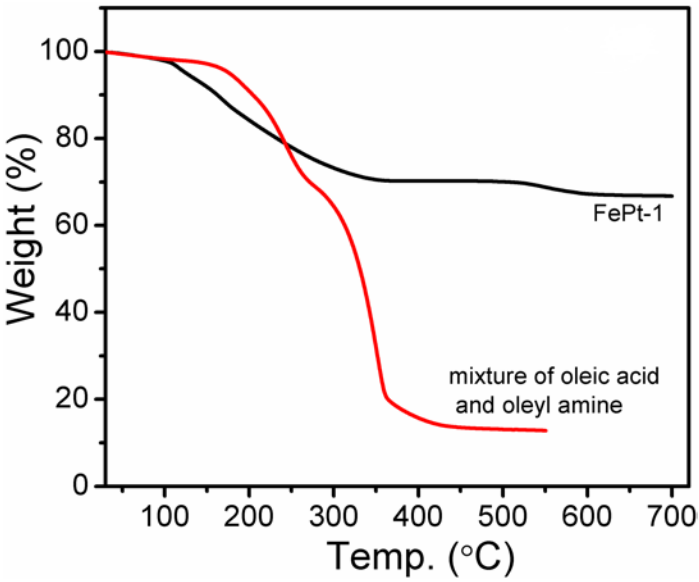

Fig. 3 TGA plots FePt-1 and surfactant (mixture of oleic acid and oleylamine in 1:1 vol%).

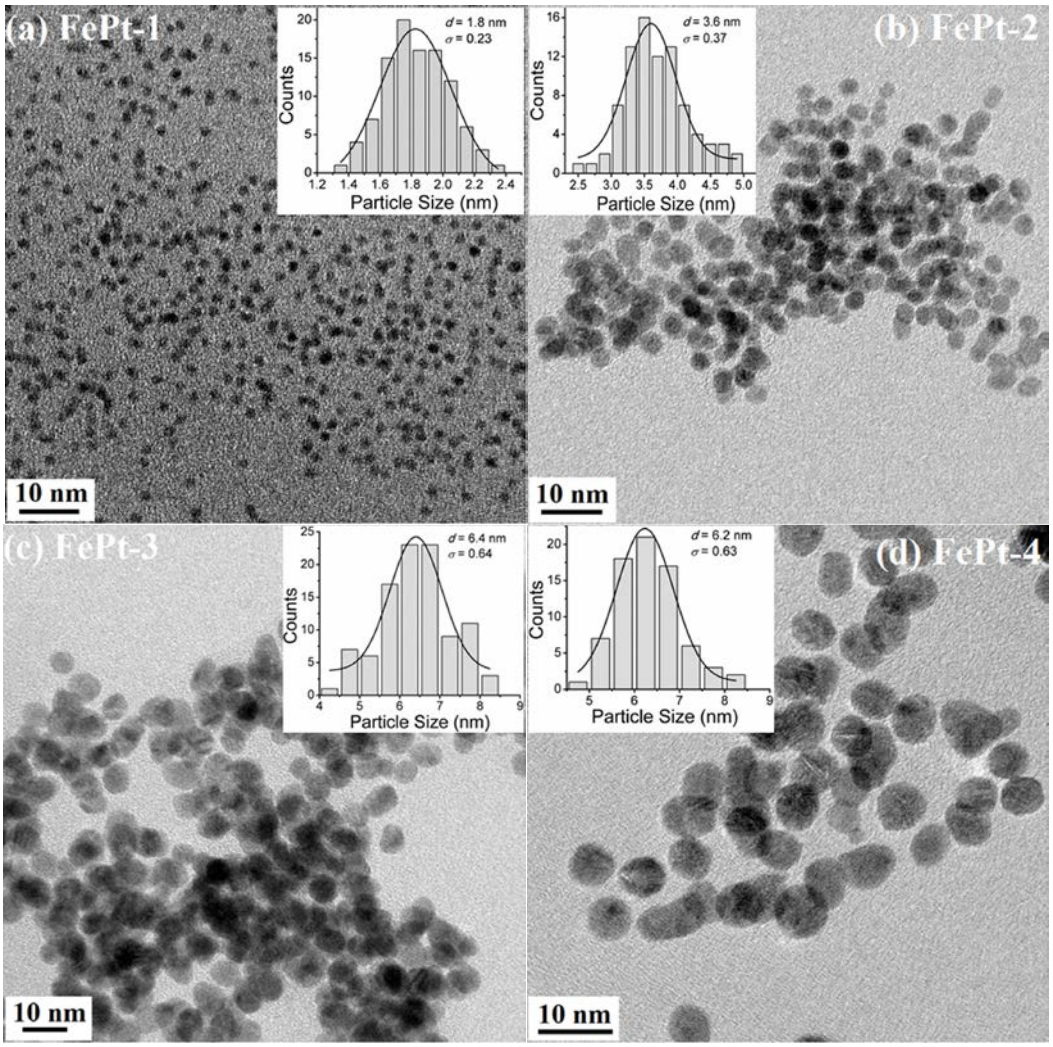

Fig. 4 TEM images of as-synthesized FePt NPs: (a) FePt-1, (b) FePt-2, (c) FePt-3, and (d) FePt-4. The particles size distributions are shown in the insets.

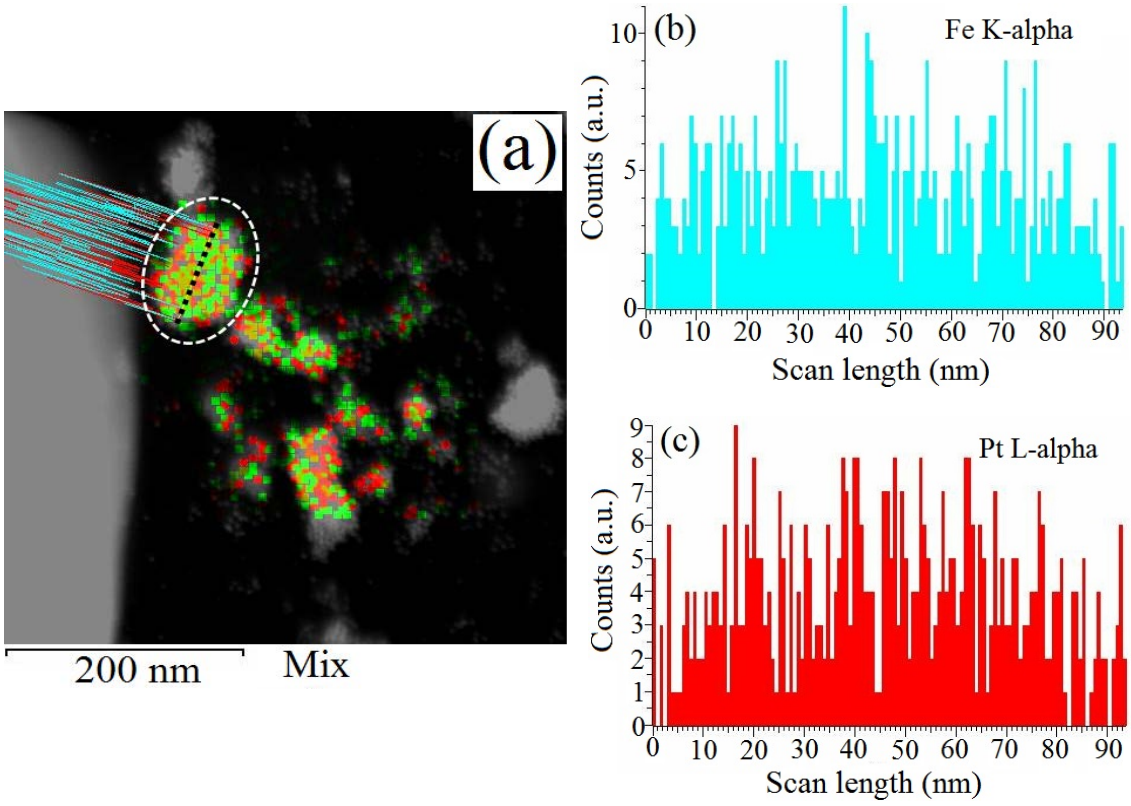

Fig. 5 (a) STEM mapping image of FePt-2 where dotted circle represents the area scan of the sample and (b, c) corresponding EDX profiles of Fe and Pt along the dotted line drawn over the sample.

Table I Details of average elemental compositions found in EDX analysis from SEM and particle size from TEM.

Sample	Fe at.%	Pt at.%	Particle size (nm)
FePt-1	45.9	54.1	2.0
FePt-2	31.5	68.5	3.6
FePt-3	24.6	75.4	6.4
FePt-4	19.1	80.9	6.2

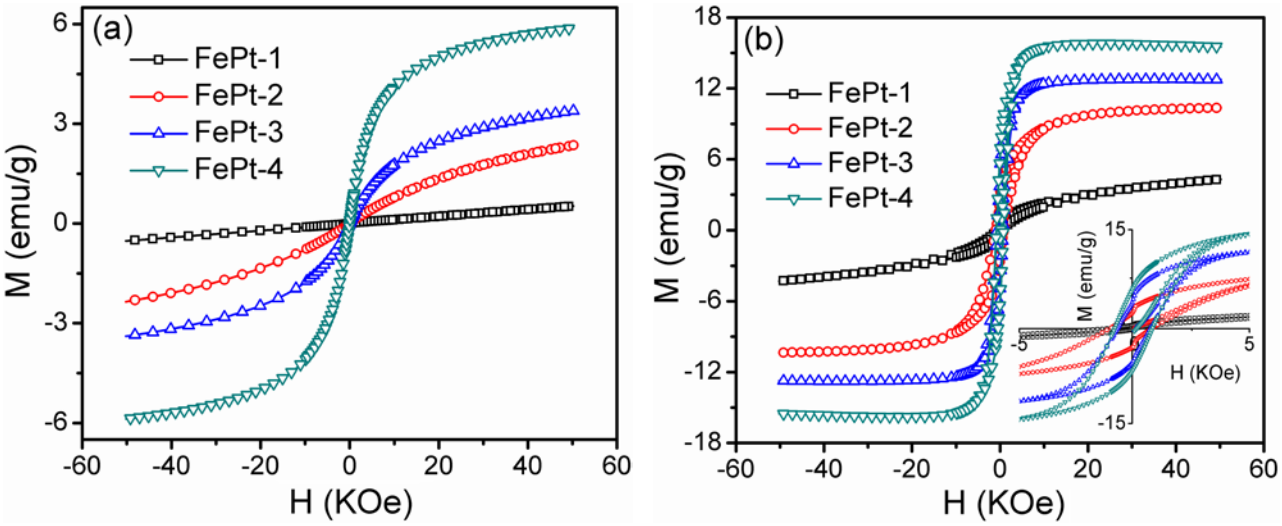

Fig. 6 *M-H* curves of as-synthesized FePt NPs measured at (a) 300 K and (b) 5 K. Applied field is from -5T to 5T. A part of the Fig. (b) is expanded and shown in the inset.

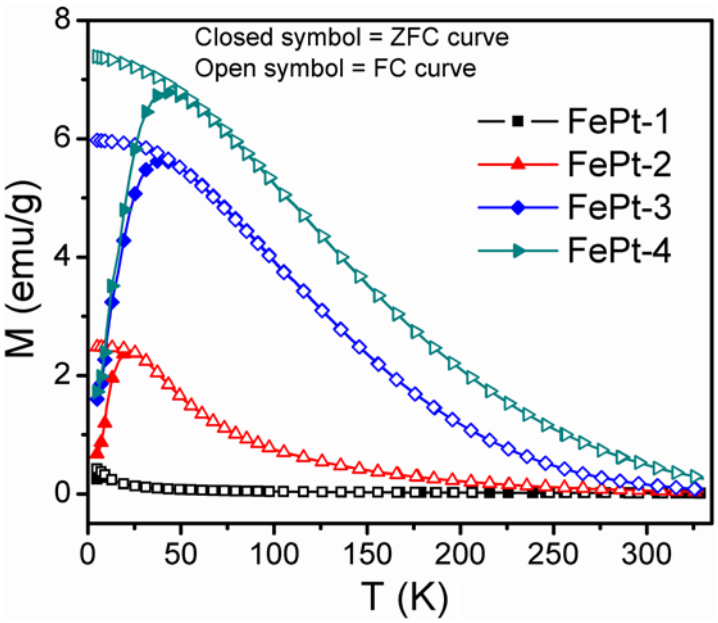

Fig. 7 *ZFC-FC* curves of as-synthesized sample at an applied field of 500 Oe.

Table II Details of the magnetic data of the as-synthesized FePt NPs measured at 300 and 5K with the applied field from -5T to 5T. M_{300K} and M_{5K} are the magnetization at 300 and 5K, respectively (H_a= 5T), Hc_{5K} is the coercivity at 5K.

Sample	T_B(K)	M_{300K} (emu/g)	M_{5K} (emu/g)	Hc_{5K}(Oe)
FePt-1	9.2	0.5	4.3	542
FePt-2	22.3	2.4	10.4	930
FePt-3	40.3	3.4	12.8	684
FePt-4	40.3	5.9	15.5	831

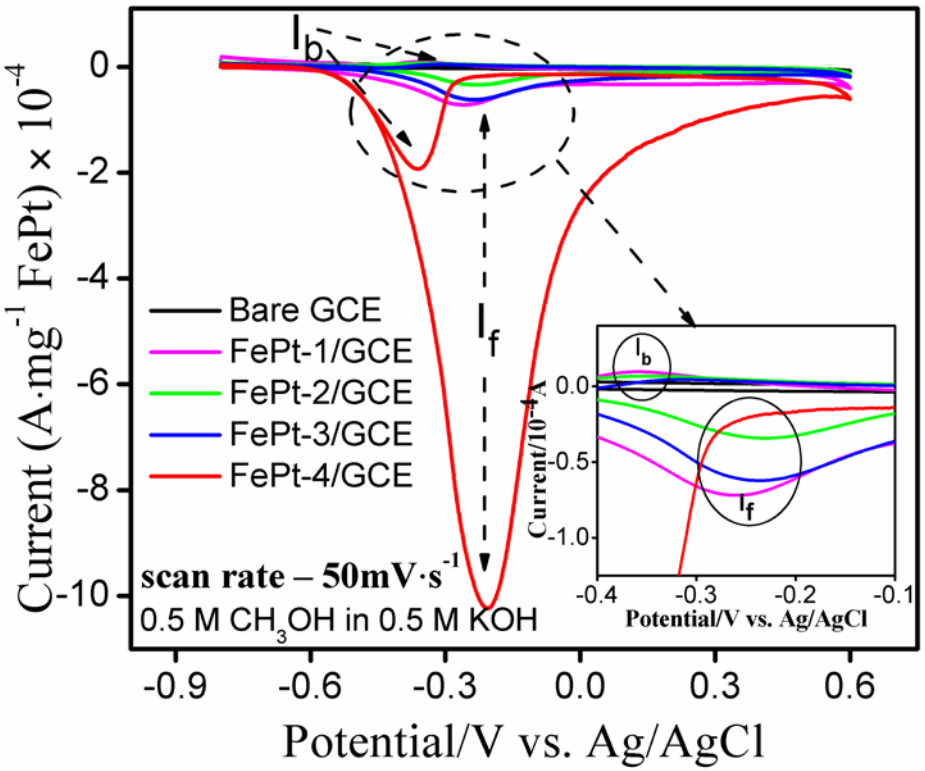

Fig. 8 Cyclic voltammograms of methanol oxidation on different FePt catalysts in solution containing 0.5 M KOH and 0.5M CH_3OH at room temperature, with a scan rate of 50 mV·s^{-1}. A part of CV responses of the materials (encircled area) is magnified and is shown in inset.

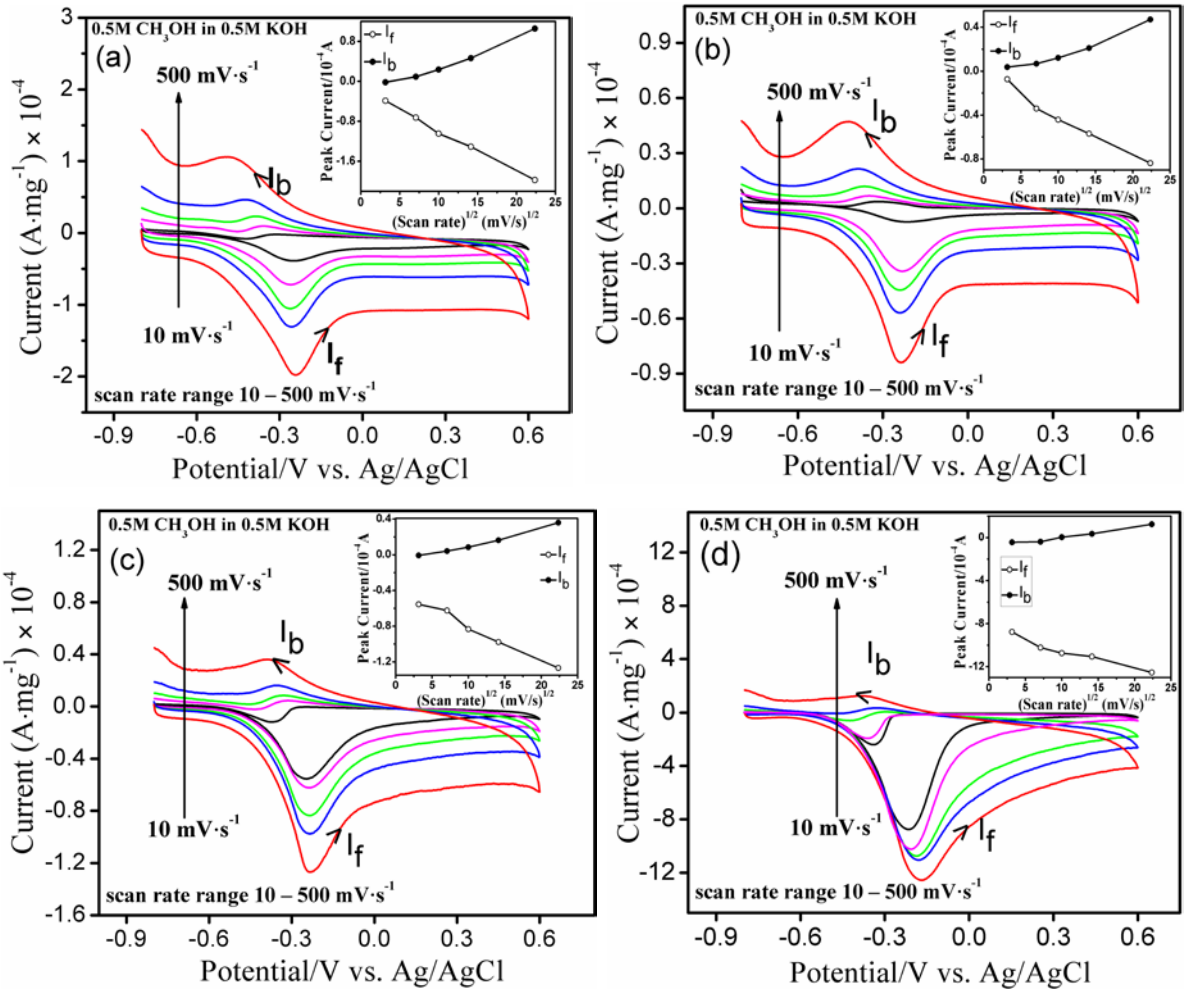

Fig. 9 Cyclic voltammograms of methanol oxidation on different FePt catalysts: (a) FePt-1, (b) FePt-2, (c) FePt-3 and (d) FePt-4 in solution containing 0.5 M KOH and 0.5M CH_3OH at room temperature with different scan rates from 10 to 500mVs^{-1}. (Insets: dependence of cathodic and anodic peak currents on square root of potential sweep rate).

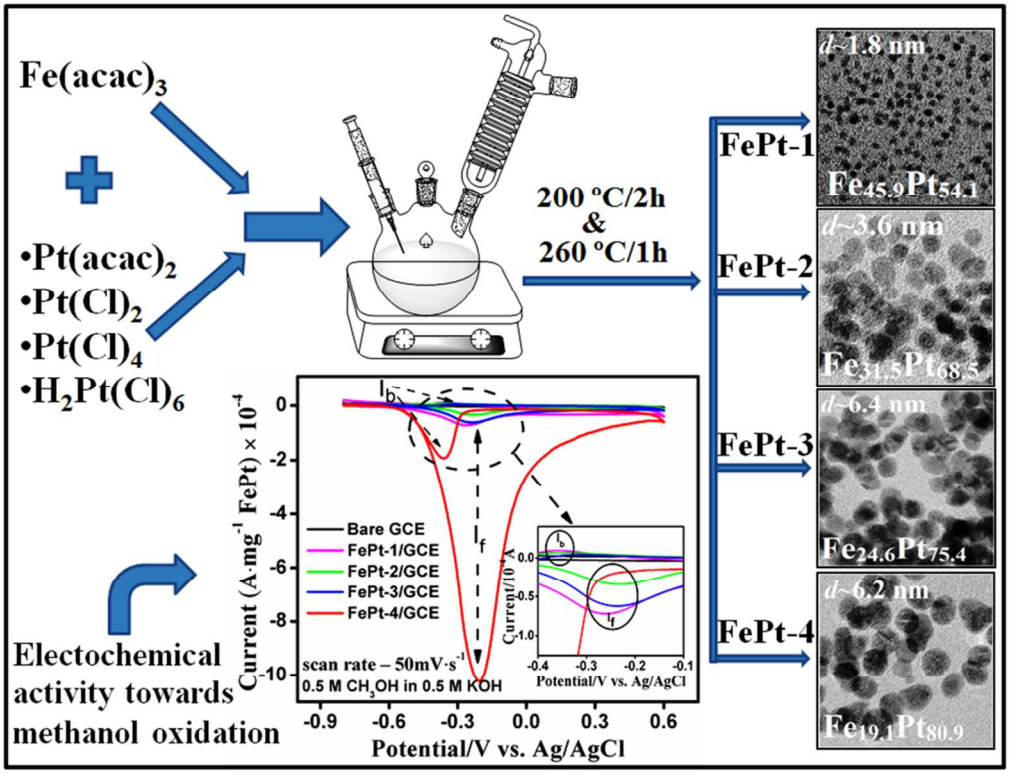

Scheme 1 Schematic representation of the formation of FePt NPs from different platinum precursors and a fixed iron precursor and their electrochemical activity towards methanol oxidation.